Frontiers of Information Technology & Electronic Engineering
www.jzus.zju.edu.cn; engineering.cae.cn; www.springerlink.com
ISSN 2095-9184 (print); ISSN 2095-9230 (online)
E-mail: jzus@zju.edu.cn

Target tracking methods based on SNR model*

Dai Liu[1,2], Yong-bo Zhao[†‡1], Zi-qiao Yuan[2], Jie-tao Li[2], Guo-ji Chen[2]

[1]*National Lab of Radar Signal Processing, Xidian University, Xi'an 710071, China*

[2]*Xi'an Electronic Engineering Research Institute, Xi'an, 710100, China*

[†]E-mail: ybzhao@xidian.edu.cn

Received Dec. 4, 2019; Revision accepted Feb. 9, 2020; Crosschecked

Abstract: In traditional target tracking methods, angle and range errors are often measured by empirical value, while observation noise is a fixed constant. Angle and range error are analyzed. They are influenced by the signal to noise ratio (SNR). Therefore, a model related to SNR has been established, in which the SNR information is applied for target tracking. Combined with an advanced non-linear filter method, the extended Kalman filter method based on the SNR model (SNR-EKF) and the Unscented Kalman filter method based on SNR model (SNR-UKF) are proposed. There is little difference between the SNR-EKF and SNR-UKF methods in position precision, but the SNR-EKF method has advantages over in computation time, and the SNR-UKF method has advantages in velocity precision. Simulation results show that target tracking methods based on the SNR model can greatly improve tracking performance compared with traditional tracking methods. The target tracking accuracy and the convergence speed of the proposed methods represent significant improvements.

Key words: SNR model; Target tracking; The angle error; The range error; Non-linear filter
https://doi.org/10.1631/FITEE.1900679 **CLC number:**

1 Introduction

With the increasing requirements of weapon systems for tracking and guiding radar, improving target tracking accuracy has become an important research topic (Tang et al., 2017; Daniyan et al., 2018; Zhang XY et al., 2019; Zhang Y et al., 2019). The current study on target tracking is mainly focused on obtaining more measurement information, a requirement of target tracking. The measurement information includes target position, velocity, radial velocity (Ehrman and Lanterman, 2008; Musicki and Song, 2013; Zhou et al., 2014), target pose (Liu et al., 2019), High Resolution Range Profile (HRRP) (Hong et al., 2004; Ruan and Hong, 2006; Du et al., 2007), Radar Cross Section (RCS) (Ehrman and Mahapatra, 2009), and target amplitude (Brekke et al., 2010; Mertens et al., 2016). These measurements have been applied to the target measurement equation to improve target tracking performance. The radial velocity has been introduced to the measurement equation of the Kalman filter to improve target tracking accuracy (Ehrman and Lanterman, 2008; Musicki and Song, 2013; Zhou et al., 2014). Two target tracking methods aided by the pose of target have been proposed to improve prediction accuracy (Liu et al., 2019). A feature-aided tracking method has been proposed, one which uses HRR features and the technique of mixture density estimation (Ruan and Hong, 2006). The high-resolution range measurement has been used for ground moving-target tracking and identification (Hong et al., 2004). Complex HRRP has been exploited to obtain better recognition results (Du et al., 2007). RCS-assisted tracking is used and is effective when targets are closely spaced (Ehrman and Mahapatra, 2009). The RCS information is exploited to improve radar performance in some

‡ Corresponding author

* Project supported by the National Natural Science Foundation of China (No. 61671357)

ORCID: Dai Liu, https://orcid.org/0000-0000-0000-0000; Yong-bo Zhao https://orcid.org/0000-0000-0000-0000

situations (Mertens et al., 2016). The amplitude information has been used to the probabilistic data association filter to improve the radar performance E. Brekke et al., 2010). The authors propose that the probabilistic data association filter with amplitude information can safely operate in the presence of very abundant clutter (Brekke et al., 2011).

With the rapid development of radar technology, it is possible to obtain the signal to noise ratio (SNR) information of the target with high precision (Das and Rao, 2012; Villano, 2014). Accurate SNR and noise variance estimation has been addressed in multiple-input multiple-output (MIMO) systems (Das and Rao, 2012). The estimation of the noise variance and SNR of the cross-polarized channels has been discussed in synthetic aperture radar (SAR) data (Villano, 2014). SNR information is applied to radar target tracking in this paper.

Compared with traditional target tracking methods, SNR information is extended to the radar target tracking method in this paper. The relationship between range error, angle error and SNR is analyzed. The SNR model is established and the measurement noise matrix in the filter method is modified. In traditional target tracking methods, angle error and range error are fixed at constant values. In contrast, the angle error and range error are varied with the SNR in the proposed methods. Combined with advanced non-linear filter methods (extended Kalman filter method (EKF) (Barczyk et al., 2015; Rashedi et al., 2018; Xi et al., 2018) and unscented Kalman filter method (UKF) (Gokce and Kuzuoglu, 2015; Liu et al., 2011; Menegaz et al., 2019), the extended Kalman filter method based on SNR model (SNR-EKF) and the unscented Kalman filter method based on SNR model (SNR-UKF) are proposed. The simulation results show that the proposed methods have higher tracking accuracy and faster convergence speed than the traditional target tracking methods.

2 Mathematical model

Assuming that the target state equation is

$$\boldsymbol{X}_k = \boldsymbol{F}_{k|k-1}\boldsymbol{X}_{k-1} + \boldsymbol{V}_{k-1}, \tag{1}$$

where $\boldsymbol{X}_k=[x_k, \dot{x}_k, y_k, \dot{y}_k, z_k, \dot{z}_k]^{\mathrm{T}}$ represents the state vector at time k, (x_k, y_k, z_k) and $(\dot{x}_k, \dot{y}_k, \dot{z}_k)$ represent the position and velocity of the target on the XYZ axis respectively at time k, $\boldsymbol{F}_{k|k-1}$ represents the target state transitional matrix, and $\boldsymbol{V}_{k-1}$ represents the process noise with state noise intensity σ_w^2 and covariance $\boldsymbol{Q}$.

$$\boldsymbol{F}_{k|k-1}=\begin{bmatrix} 1 & T & 0 & 0 & 0 & 0 \\ 0 & 1 & 0 & 0 & 0 & 0 \\ 0 & 0 & 1 & T & 0 & 0 \\ 0 & 0 & 0 & 1 & 0 & 0 \\ 0 & 0 & 0 & 0 & 1 & T \\ 0 & 0 & 0 & 0 & 0 & 1 \end{bmatrix}$$

$$\boldsymbol{Q}=\sigma_w^2\begin{bmatrix} \frac{T^3}{3} & \frac{T^2}{2} & 0 & 0 & 0 & 0 \\ \frac{T^2}{2} & T & 0 & 0 & 0 & 0 \\ 0 & 0 & \frac{T^3}{3} & \frac{T^2}{2} & 0 & 0 \\ 0 & 0 & \frac{T^2}{2} & T & 0 & 0 \\ 0 & 0 & 0 & 0 & \frac{T^3}{3} & \frac{T^2}{2} \\ 0 & 0 & 0 & 0 & \frac{T^2}{2} & T \end{bmatrix}$$

The "T" in the matrix refers to the sampling interval.

Suppose that the target's measurement equation is

$$\boldsymbol{Z}_k = \boldsymbol{h}(\boldsymbol{X}_k) + \boldsymbol{W}_k, \tag{2}$$

where $\boldsymbol{Z}_k$ represents the measurements at time k, $\boldsymbol{h}(\cdot)$ represents the measurement function, and $\boldsymbol{W}_k$ represents the measurement noise at time k.

The variance of measurement noise is given as

$$E[\boldsymbol{W}_k\boldsymbol{W}_j^{\mathrm{T}}] = \boldsymbol{R}_k\delta_{kj},$$

$$\delta_{kj}=\begin{cases}1, & k=j,\\ 0, & k\neq j.\end{cases}$$

If $\boldsymbol{Z}_k=[\rho_k, \theta_k, \varphi_k]$,

$$\boldsymbol{h}(x_k)=\begin{bmatrix}\sqrt{x_k^2+y_k^2+z_k^2}\\ \arctan(y_k/x_k)\\ \arctan(z_k/\sqrt{x_k^2+y_k^2})\end{bmatrix}$$

$$\boldsymbol{R}_k=\begin{bmatrix}\sigma_{\rho_k}^2 & 0 & 0\\ 0 & \sigma_{\theta_k}^2 & 0\\ 0 & 0 & \sigma_{\varphi_k}^2\end{bmatrix}$$

If $\boldsymbol{Z}_k=[x_k, y_k, z_k]$,

$$\boldsymbol{h}(\boldsymbol{X}_k)=\begin{bmatrix}x_k\\ y_k\\ z_k\end{bmatrix},$$

$$\boldsymbol{R}_k=\boldsymbol{A}\begin{bmatrix}\sigma_{\rho_k}^2 & 0 & 0\\ 0 & \sigma_{\theta_k}^2 & 0\\ 0 & 0 & \sigma_{\varphi_k}^2\end{bmatrix}\boldsymbol{A}^{\mathrm{T}},$$

$$\boldsymbol{A}=\begin{bmatrix}\cos\theta_k\cos\varphi_k & -\rho_k\sin\theta_k\cos\varphi_k & -\rho_k\cos\theta_k\sin\varphi_k\\ \sin\theta_k\cos\varphi_k & \rho_k\cos\theta_k\cos\varphi_k & -\rho_k\sin\theta_k\sin\varphi_k\\ \sin\varphi_k & 0 & \rho_k\cos\varphi_k\end{bmatrix},$$

where $(\rho_k, \theta_k, \varphi_k)$ represents the range, azimuth and elevation of the target in the polar coordinate system at time k, (x_k, y_k, z_k) represents the position of the target in the Cartesian coordinate system at time k, $\sigma_{\rho_k}^2$ represents the variance of range measurement error at time k, $\sigma_{\theta_k}^2$ represents the variance of azimuth measurement error at time k, and $\sigma_{\varphi_k}^2$ represents the variance of elevation measurement error at time k. This paper adopts $\boldsymbol{Z}_k=[\rho_k, \theta_k, \varphi_k]$ for the convenience of analysis. In traditional target tracking methods, $\sigma_{\rho_k}^2$, $\sigma_{\theta_k}^2$, and $\sigma_{\varphi_k}^2$ are the empirical values for fixed constants.

3 Target tracking methods based on SNR model

3.1 SNR analysis

The expression between the minimum detection SNR and the range can be described as (Skolnik, 2010)

$$(\mathrm{SNR})_{\min}=\frac{P_{\mathrm{t}}G_{\mathrm{t}}G_{\mathrm{r}}\lambda^2\sigma}{(4\pi)^3\mathrm{k}_1T_0BFLR^4},\tag{3}$$

where $(\mathrm{SNR})_{\min}$ denotes the minimum detection SNR, R denotes the target range, P_{t} denotes the average power of the transmitter, G_{t} denotes the transmit gain of the antenna, G_{r} denotes the receive gain of the antenna, λ denotes the wavelength, σ denotes RCS of target, B denotes the receiver bandwidth, F denotes the receiver noise coefficient, L denotes the radar loss, k_1 denotes the Boltzmann constant, and T_0 denotes standard room temperature.

Suppose that σ is 0.1 m^2, 1 m^2 and 10 m^2 respectively, while P_{t}=1500 W, λ=0.0536 m, G_t=45, G_r=45, B=5×10^6 Hz, F=3, L=6. As shown in Fig. 1, the SNR varies with range. It can be seen from the figure that SNR decreases with the increase of target range and increases with the decrease of target range. At the same range, the larger the RCS of the target is, the larger the SNR of the target is.

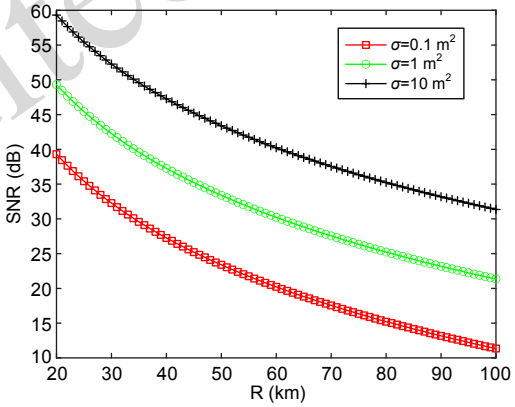

Fig. 1 SNR variation curve with range

3.2 Angle error analysis

The angle error caused by the thermal noise of the receiver is described as

$$\sigma_{\phi 1}=\frac{\mathrm{BW}}{K_{\mathrm{m}}\sqrt{2\mathrm{SNR}}},\tag{4}$$

where BW denotes 3 dB beam width, K_{m} denotes single pulse angle slope, and SNR denotes the signal to noise ratio.

As shown in Fig. 2, angle error varies with SNR when K_{m}=1.5 and BW is 1°, 2°, and 3°, respectively. It can be seen from the figure that angle error caused

by thermal noise of the receiver depends on the antenna beam width and SNR. Under the same antenna beam width, the larger the SNR of the target, the smaller the angle error caused by the thermal noise of receiver. With the same SNR condition, the narrower the antenna beam width, the smaller the angle error caused by the thermal noise of receiver.

In fact, the angle error of radar is not only related to the thermal noise of receiver, but also affected by factors such as angular glint, quantization error of angle coding, sampling quantization error, amplitude-phase imbalance, atmospheric refraction, etc. However, the thermal noise of the receiver is the main factor resulting in angle error. Assume that the angle error caused by other factors except the thermal noise of receiver is $\sigma_{\phi 2}$.

Because $\sigma_{\phi 1}$ and $\sigma_{\phi 2}$ are independent, there exists

$$\sigma_{\phi}^2=\sigma_{\phi 1}^2+\sigma_{\phi 2}^2. \tag{5}$$

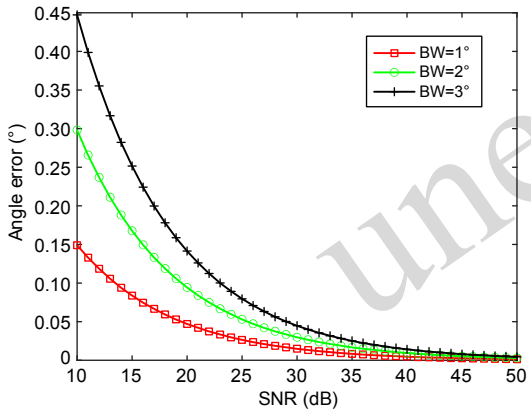

Fig. 2 Angle error variation curve with SNR

3.3 Range error analysis

The range error caused by the thermal noise of the receiver is described as follows:

$$\sigma_{\rho 1}=\frac{c}{2B\sqrt{2SNR}}, \tag{6}$$

where B is the signal bandwidth, and c is the propagation speed of the electromagnetic wave.

As shown in Fig. 3, range error varies with SNR when B is 3 M, 6 M and 9 M, respectively. It can be seen from the figure that range error caused by thermal noise of the receiver depends on the signal bandwidth and SNR. With the same signal bandwidth, the larger the SNR of target, the smaller the range error caused by the thermal noise of the receiver. With the same SNR condition, the larger the signal bandwidth, the smaller the range error caused by the thermal noise of the receiver.

In fact, the range error of the radar is not only related to the thermal noise of the receiver, but is also affected by factors such as angular glint, range quantization error, multipath, transmitted pulse jitter, range Doppler coupling, atmospheric refraction, etc. Assume that the range error caused by factors other than the thermal noise of the receiver is $\sigma_{\rho 2}$.

Because $\sigma_{\rho 1}$ and $\sigma_{\rho 2}$ are independent, there exists

$$\sigma_{\rho}^2=\sigma_{\rho 1}^2+\sigma_{\rho 2}^2. \tag{7}$$

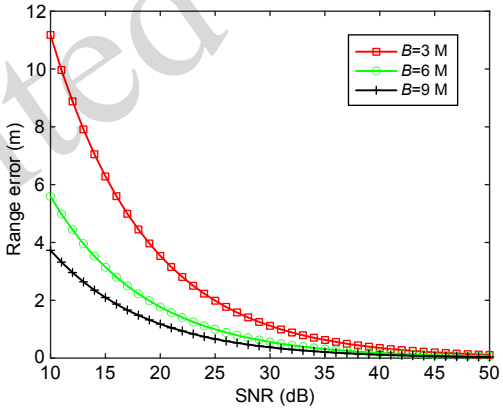

Fig. 3 Range error variation curve with SNR

3.4 Target tracking methods based on SNR model

3.4.1 Selection of measurement noise covariance

Minimum SNR is calculated according to the detection probability and false alarm probability determined by radar (Alberhseim, 1981; Tufts and Cann, 1983):

$$(\mathrm{SNR})_{\min}=A+0.12AB+1.7B, \tag{8}$$

where A=ln(0.62/P_{fa}), B=ln(P_{d}/(1−P_{d})). P_{fa} denotes false alarm probability, and P_{d} denotes detection probability.

Assume the target SNR at time k is $(\mathrm{SNR})_k$, then $(\mathrm{SNR})_k>(\mathrm{SNR})_{\min}$. According to Eqs. (4)–(7), the

measurement noise covariance at time k in polar coordinates can be obtained as follows:

$$\begin{aligned}\boldsymbol{R}_k &= \begin{bmatrix}\sigma_{\rho_k}^2 & 0 & 0\\ 0 & \sigma_{\theta_k}^2 & 0\\ 0 & 0 & \sigma_{\varphi_k}^2\end{bmatrix}\\ &= \begin{bmatrix}\sigma_{\rho 1_k}^2+\sigma_{\rho 2_k}^2 & 0 & 0\\ 0 & \sigma_{\theta 1_k}^2+\sigma_{\theta 2_k}^2 & 0\\ 0 & 0 & \sigma_{\varphi 1_k}^2+\sigma_{\varphi 2_k}^2\end{bmatrix}\\ &= \begin{bmatrix}\sigma_{\rho 1_k}^2 & 0 & 0\\ 0 & \sigma_{\theta 1_k}^2 & 0\\ 0 & 0 & \sigma_{\varphi 1_k}^2\end{bmatrix}+\begin{bmatrix}\sigma_{\rho 2_k}^2 & 0 & 0\\ 0 & \sigma_{\theta 2_k}^2 & 0\\ 0 & 0 & \sigma_{\varphi 2_k}^2\end{bmatrix}\\ &= \begin{bmatrix}\dfrac{c^2}{8B^2(\mathrm{SNR})_k} & 0 & 0\\ 0 & \dfrac{\theta_{\mathrm{H}}{}^2}{2\mathrm{K_m}{}^2(\mathrm{SNR})_k} & 0\\ 0 & 0 & \dfrac{\varphi_{\mathrm{H}}{}^2}{2\mathrm{K_m}{}^2(\mathrm{SNR})_k}\end{bmatrix}\\ &\quad+\begin{bmatrix}\sigma_{\rho 2_k}^2 & 0 & 0\\ 0 & \sigma_{\theta 2_k}^2 & 0\\ 0 & 0 & \sigma_{\varphi 2_k}^2\end{bmatrix}\\ &= \boldsymbol{R}_{k1}+\boldsymbol{R}_{k2},\end{aligned} \tag{9}$$

where θ_{H} denotes the azimuth 3 dB beam width, and φ_{H} denotes the elevation 3 dB beam width.

$$\boldsymbol{R}_{k1} = \begin{bmatrix}\dfrac{c^2}{8B^2(\mathrm{SNR})_k} & 0 & 0\\ 0 & \dfrac{\theta_{\mathrm{H}}{}^2}{2\mathrm{K_m}{}^2(\mathrm{SNR})_k} & 0\\ 0 & 0 & \dfrac{\varphi_{\mathrm{H}}{}^2}{2\mathrm{K_m}{}^2(\mathrm{SNR})_k}\end{bmatrix} \tag{10}$$

$\boldsymbol{R}_{k1}$ denotes the measurement noise covariance caused by the thermal noise of the receiver.

$\boldsymbol{R}_{k2}$ denotes the measurement noise covariance caused by factors other than the thermal noise of the receiver.

3.4.2 Extended Kalman filter method based on SNR model

The SNR-EKF method applies the target SNR information to the EKF method. Suppose that the target state and the covariance matrix are respectively $\hat{\boldsymbol{X}}_{k-1|k-1}$, $\boldsymbol{P}_{k-1|k-1}$ at time $k-1$, $\boldsymbol{z}_k=[\rho_k, \theta_k, \varphi_k]^{\mathrm{T}}$, $(\mathrm{SNR})_k$ is the target SNR at time k, $\boldsymbol{R}_{k2}$ is the measurement noise covariance caused by factors other than the thermal noise of the receiver at time k, The detailed steps of the SNR-EKF method are as follows:

Step 1: Judge whether $(\mathrm{SNR})_k$ satisfies the condition of $(\mathrm{SNR})_k \geq (\mathrm{SNR})_{\min}$. If it does, turn to Step 2.

Step 2: Calculate $\boldsymbol{R}_{k1}$ according to Eq. (10), and then substitute it into Eq. (9) to get $\boldsymbol{R}_k$.

Step 3: State prediction.

$$\hat{\boldsymbol{X}}_{k|k-1} = \boldsymbol{F}\hat{\boldsymbol{X}}_{k-1|k-1}, \tag{11}$$

$$\boldsymbol{P}_{k|k-1} = \boldsymbol{F}\boldsymbol{P}_{k-1|k-1}\boldsymbol{F}^{\mathrm{T}} + \boldsymbol{Q}_{k-1}. \tag{12}$$

Step 4: State update.

$$\boldsymbol{K}_k = \boldsymbol{P}_{k|k-1}\boldsymbol{H}_k\boldsymbol{S}_k^{-1}, \tag{13}$$

$$\hat{\boldsymbol{X}}_{k|k} = \hat{\boldsymbol{X}}_{k|k-1} + \boldsymbol{K}_k(\boldsymbol{z}_k - h(\hat{\boldsymbol{X}}_{k|k-1})), \tag{14}$$

$$\boldsymbol{P}_{k|k} = [\boldsymbol{I}-\boldsymbol{K}_k\boldsymbol{H}_k]\boldsymbol{P}_{k|k-1}[\boldsymbol{I}-\boldsymbol{K}_k\boldsymbol{H}_k]^{\mathrm{T}} - \boldsymbol{K}_k\boldsymbol{R}_k\boldsymbol{K}_k^{\mathrm{T}}, \tag{15}$$

where $\boldsymbol{H}_k = (\Delta_{x_k} h^{\mathrm{T}}(\boldsymbol{X}_k))^{\mathrm{T}}$, $\boldsymbol{S}_k = \boldsymbol{H}_k\boldsymbol{P}_{k|k-1}\boldsymbol{H}_k^{\mathrm{T}} + \boldsymbol{R}_k$.

3.4.3 Unscented Kalman filter method based on SNR model

The SNR-UKF method applies the target SNR information to the UKF method. The assumption of the SNR-UKF method is the same as the SNR-EKF method. The detailed steps of the SNR-UKF method are as follows:

Step 1: Judge whether $(\mathrm{SNR})_k$ satisfies the condition of $(\mathrm{SNR})_k \geq (\mathrm{SNR})_{\min}$. If it does, turn to Step 2.

Step 2: Calculate $\boldsymbol{R}_{k1}$ according to Eq. (10), and then substitute it into Eq. (9) to get $\boldsymbol{R}_k$.

Step 3: Time update.

$$\begin{cases}\boldsymbol{\chi}_{k-1|k-1}^0 = \hat{\boldsymbol{X}}_{k-1|k-1},\\ \boldsymbol{\chi}_{k-1|k-1}^i = \hat{\boldsymbol{X}}_{k-1|k-1} + \left(\sqrt{(n+\lambda)\boldsymbol{P}_{k-1|k-1}}\right), i=1,2,\ldots,n,\\ \boldsymbol{\chi}_{k-1|k-1}^i = \hat{\boldsymbol{X}}_{k-1|k-1} - \left(\sqrt{(n+\lambda)\boldsymbol{P}_{k-1|k-1}}\right),\\ \qquad\qquad i=n+1,n+2,\ldots,2n,\end{cases} \tag{16}$$

$$\begin{cases} \omega_0^m = \dfrac{\kappa}{n+\kappa}, \\ \omega_0^c = \dfrac{\kappa}{n+\kappa} + 1 - \alpha^2 + \gamma, \\ \omega_i^m = \omega_i^c = \dfrac{\kappa}{2(n+\kappa)}, i = 1, 2, ..., 2n, \end{cases} \tag{17}$$

$$\boldsymbol{\chi}_{k|k-1}^i = \boldsymbol{F}\boldsymbol{\chi}_{k-1|k-1}^i, \tag{18}$$

$$\hat{\boldsymbol{X}}_{k|k-1} = \sum_{i=0}^{2n} \omega_i^m \boldsymbol{\chi}_{k|k-1}^i, \tag{19}$$

$$\boldsymbol{P}_{k|k-1} = \sum_{i=0}^{2n} \omega_i^c (\boldsymbol{\chi}_{k|k-1}^i - \hat{\boldsymbol{X}}_{k|k-1})(\boldsymbol{\chi}_{k|k-1}^i - \hat{\boldsymbol{X}}_{k|k-1})^{\mathrm{T}} + \boldsymbol{Q}_{k-1}. \tag{20}$$

Step 4: Measurement update.

$$\boldsymbol{\xi}_{k|k-1}^i = \boldsymbol{h}(\boldsymbol{\chi}_{k|k-1}^i), \tag{21}$$

$$\hat{\boldsymbol{z}}_{k|k-1} = \sum_{i=0}^{2n} \omega_i^m \boldsymbol{\xi}_{k|k-1}^i, \tag{22}$$

$$\boldsymbol{P}_{z_k} = \sum_{i=0}^{2n} \omega_i^c (\boldsymbol{\xi}_{k|k-1}^i - \hat{\boldsymbol{z}}_{k|k-1})(\boldsymbol{\xi}_{k|k-1}^i - \hat{\boldsymbol{z}}_{k|k-1})^{\mathrm{T}} + \boldsymbol{R}_k, \tag{23}$$

$$\boldsymbol{P}_{x_k z_k} = \sum_{i=0}^{2n} \omega_i^c (\boldsymbol{\chi}_{k|k-1}^i - \hat{\boldsymbol{X}}_{k|k-1})(\boldsymbol{\xi}_{k|k-1}^i - \hat{\boldsymbol{z}}_{k|k-1})^{\mathrm{T}}. \tag{24}$$

Step 5: Filter update.

$$\boldsymbol{K}_k = \boldsymbol{P}_{z_k} \boldsymbol{P}_{x_k z_k}^{-1}, \tag{25}$$

$$\hat{\boldsymbol{X}}_{k|k} = \hat{\boldsymbol{X}}_{k|k-1} + \boldsymbol{K}_k (\boldsymbol{z}_k - \hat{\boldsymbol{z}}_{k|k-1}), \tag{26}$$

$$\boldsymbol{P}_{k|k} = \boldsymbol{P}_{k|k-1} - \boldsymbol{K}_k \boldsymbol{P}_{z_k} \boldsymbol{K}_k^{\mathrm{T}}. \tag{27}$$

4 Simulations and analysis

In order to verify the effectiveness of the proposed method, the simulation has been conducted as follows: the target keeps 1000 m from the initial position (10 000 m, 10 000 m, 1000 m), and moves in a uniform straight line at a speed of (100 m/s, −120 m/s). The target trajectory is shown in Fig. 4. The radar system parameters are as follows: P_t=5000 W, λ=0.056 m, G_t=45, G_r=45, B=5×10^6 Hz, F=3, L=6, σ=0.1 m^2, P_d=50%, P_{fa} =10^{-6}, $\sigma_{\rho 2}$=15m, $\sigma_{\phi 2}$=0.0286°. Bringing P_d and P_{fa} into Eq. (8), there exists $(\mathrm{SNR})_{\min}$=13.3 dB. Two hundred Monte Carlo experiments have been carried out with the observation data interval of 1 s and duration of 100 s. The process noise is white noise with a mean value of 0 and state noise intensity of 1.

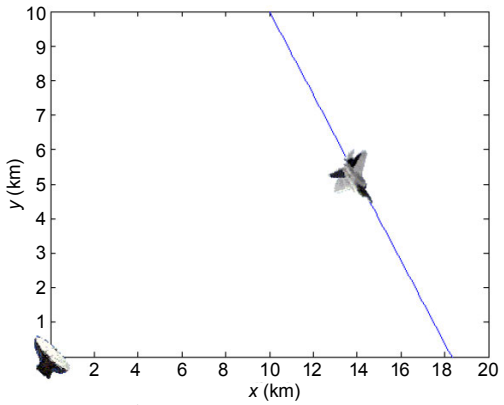

Fig. 4 Trajectory of the target

Three scenarios are simulated here. Scenario 1: range error remains unchanged at 30 m, and the angle error is varied with SNR. This scenario is designed to verify the effect of SNR on angle error and target tracking performance. Scenario 2: angle error remains unchanged at 0.0432°, and range error varies with SNR. This scenario is designed to verify the effect of SNR on range error and target tracking performance. Scenario 3: Angle error and range error vary with SNR. This scenario is designed to verify the effect of SNR on range error, angle error and target tracking performance. The range error of the EKF method and the UKF method is 30 m, and the angle error is 0.0432°.

The SNR-EKF method, the SNR-UKF method, the traditional EKF method and the traditional UKF method are compared in the following four aspects: position precision, velocity precision, convergence speed and computation time.

The root mean square errors (RMSEs) of the target position and target velocity are as follows:

$$\mathrm{RMSE}_{pk} = \sqrt{\frac{1}{M}\sum_{i=1}^{M}[(x_k - x_k^i)^2 + (y_k - y_k^i)^2]} \tag{28}$$

$$\mathrm{RMSE}_{vk} = \sqrt{\frac{1}{M}\sum_{i=1}^{M}[(\dot{x}_k - \dot{x}_k^i)^2 + (\dot{y}_k - \dot{y}_k^i)^2]} \tag{29}$$

where M is the experiment times, $(\dot{x}_k^i, \dot{y}_k^i)$ is the

estimated target position, and $(\dot{x}_k^i, \dot{y}_k^i)$ is the estimated target velocity in the i^{th} experiment.

According to radar parameters and target route, the SNR variation can be obtained using Eq. (3). As shown in Fig. 5, with the increase of target range, the target SNR decreases from 40.52 dB to 34.53 dB. Azimuth error is generated by Eq. (4) and range error is generated by Eq. (6) in real time. From the angle error curve of Fig. 6, it can be seen that with the increase of target range, the angle error increases from 0.0384° to 0.0481°. From the range error curve in Fig. 7, it can be seen that with the increase of target range, the range error increases from 25 m to 34.9 m.

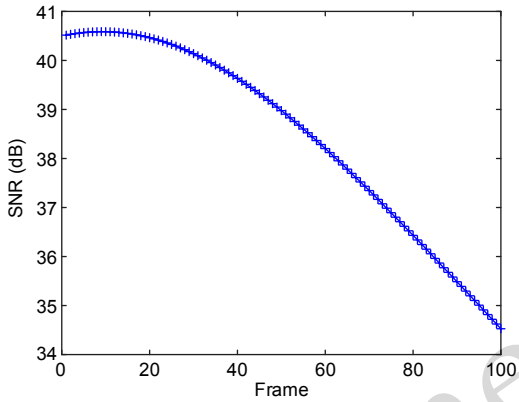

Fig. 5 SNR variation curve

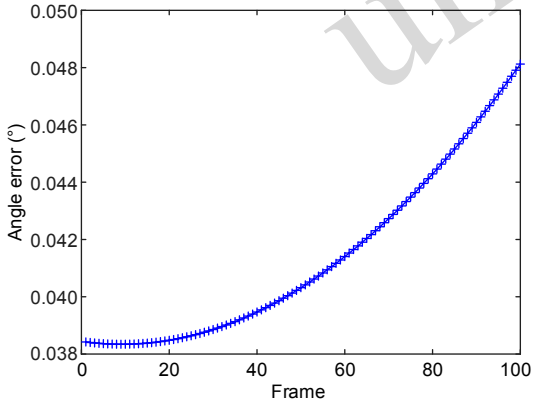

Fig. 6 Angle error curve

Scenario 1: The simulation results are shown in Figs. 8–10.

From Fig. 8, we can see that the RMSE of the target position of the traditional EKF method and the UKF method is 38.7 m, while the RMSE of the target position of the SNR-UKF method and the SNR-EKF method is 29.7 m, and the position accuracy is improved by 9 m. Compared with the traditional EKF

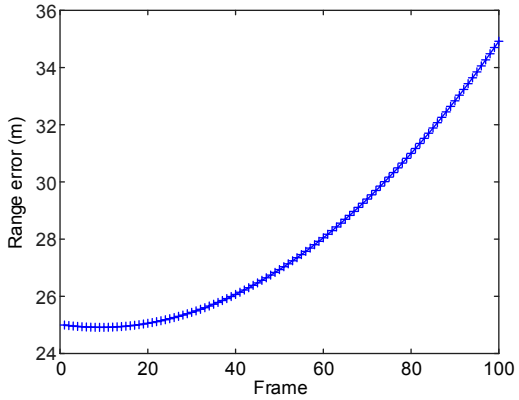

Fig. 7 Range error curve

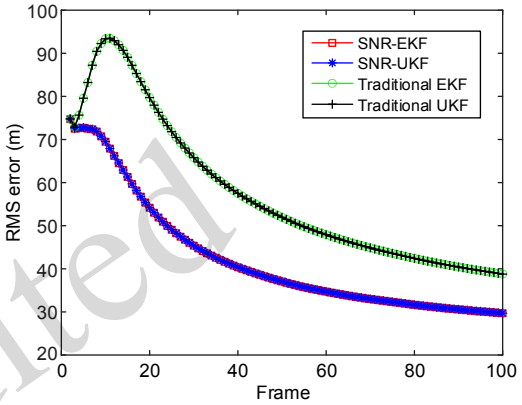

Fig. 8 RMSE of target position

method and the UKF method, the SNR-UKF method and the SNR-EKF method converge faster and have higher position accuracy. The performance of the SNR-UKF method is similar to that of the SNR-EKF method.

From Fig. 9, it can be seen that the RMSE of the target velocity of the SNR-UKF method is 22.6 m/s, that of traditional UKF method is 23.1 m/s, that of the SNR-EKF method is 31.98 m/s, and that of the traditional EKF method is 32.49 m/s. The velocity accuracy of the SNR-UKF method is 9.89 m/s higher than that of the traditional EKF method. The RMSE of the target velocity of the SNR-UKF method is the smallest and the velocity accuracy of the SNR-UKF method is the highest.

Fig. 10 shows that the computation time of the SNR-EKF and the traditional EKF method is maintained at 64 us, while that of the SNR-UKF method and the traditional UKF method is maintained at 153 us. The SNR-EKF method and the traditional EKF method are the best on computation time. Compared with the SNR-UKF method, the SNR-EKF method is

better on computation time.

From Figs. 8 and 9, it can be seen that the EKF method and the UKF method are sensitive to the value of the angle error. The angle error matching with the target SNR is conducive to improving performance.

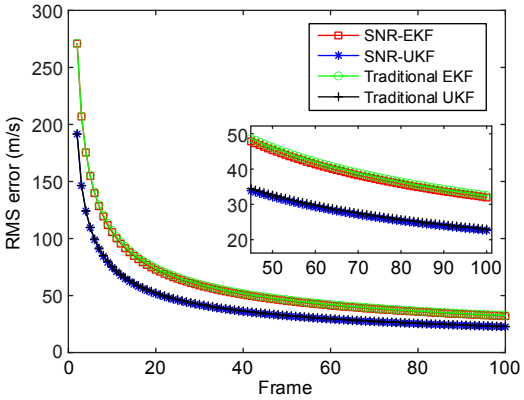

Fig. 9 RMSE of target velocity

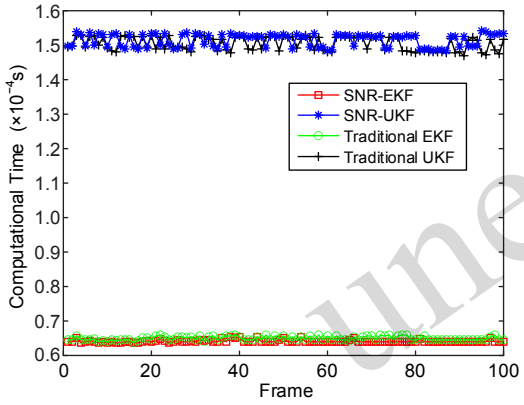

Fig. 10 The computational time of four methods

Scenario 2: The simulation results are shown in Figs. 11–13.

From Fig. 11, we can see that the RMSE of the target position of the traditional EKF method and UKF method is 35.0 m, while the RMSE of the target position of the SNR-UKF method and the SNR-EKF method is 27.0 m, and the position accuracy is improved by 8.0 m. Compared with the traditional EKF method and the UKF method, the SNR-UKF method and the SNR-EKF method converge faster and have higher position accuracy. The performance of the SNR-UKF method is similar to that of the SNR-EKF method.

From Fig. 12, it can be seen that the RMSE of the target velocity of the SNR-UKF method is 22.74 m/s, that of the traditional UKF method is 22.86 m/s, that of the SNR-EKF method is 31.88 m/s, and that of the traditional EKF method is 32.32 m/s. The velocity accuracy of the SNR-UKF method is 9.58 m/s higher than that of the traditional EKF method. The RMSE of the target velocity of the SNR-UKF method is the smallest and the velocity accuracy of the SNR-UKF method is the highest.

Fig. 13 shows that the computation time of the SNR-EKF and the traditional EKF method is maintained at 63 us, while that of the SNR-UKF method

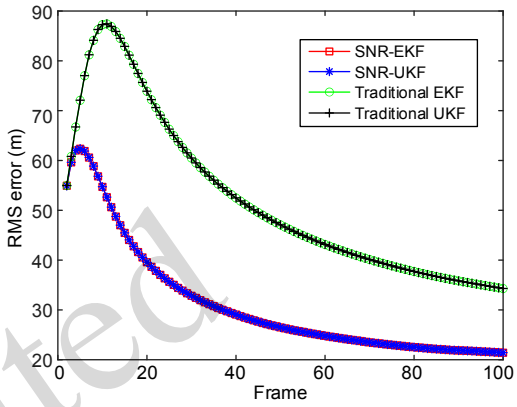

Fig. 11 RMSE of target position

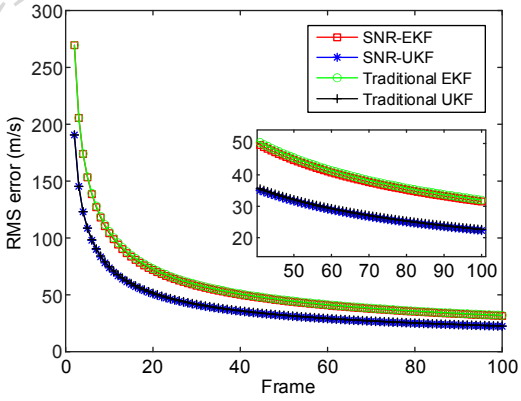

Fig. 12 RMSE of target velocity

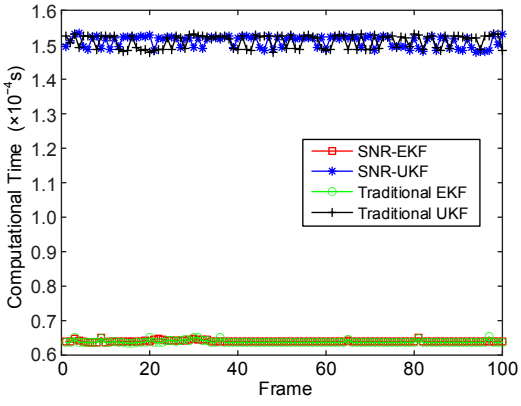

Fig. 13 The computational time of four methods

and the traditional UKF method are maintained at 152 us. The SNR-EKF and the traditional EKF method are the best on computation time. Compared with the SNR-UKF method, the SNR-EKF method is better on computation time.

From Figs. 11 and 12, it can be seen that the EKF method and the UKF method are sensitive to the value of the range error. The range error matching with the target SNR is conducive to improving performance.

Scenario 3 The simulation results are shown in Figs. 14–16.

From Fig. 14, we can see that the RMSE of the target position of the traditional EKF method and the UKF method is 34.4 m, while the RMSE of the target position of the SNR-UKF method and the SNR-EKF method is 21.4 m, which means that the position accuracy is improved by 13 m. Compared with the traditional EKF method and UKF method, the SNR-UKF method and the SNR-EKF method converge faster and have higher position accuracy. The performance of the SNR-UKF method is similar to that of the SNR-EKF method.

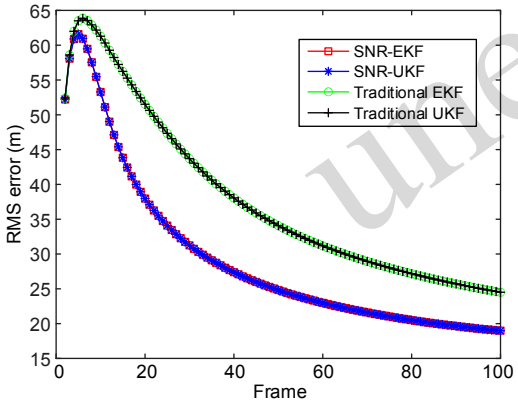

Fig. 14 RMSE of target position

From Fig. 15, it can be seen that the RMSE of the target velocity of the SNR-UKF method is 22.29 m/s, that of the traditional UKF method is 22.74 m/s, that of the SNR-EKF method is 31.53 m/s, and that of the traditional EKF method is 32.16 m/s. The velocity accuracy of the SNR-UKF method is 9.87 m/s higher than that of the traditional EKF method. The RMSE of the target velocity of the SNR-UKF method is the smallest and the velocity accuracy of the SNR-UKF method is the highest.

Fig. 16 shows that the computation time of the SNR-EKF method and the traditional EKF method is maintained at 65 us, while that of the SNR-UKF method and the traditional UKF method is maintained at 153 us. The SNR-EKF and the traditional EKF method are the best on computation time. Compared with the SNR-UKF method, the SNR-EKF method is better on computation time.

From Figs. 14 and 15, it can be seen that the EKF method and the UKF method are sensitive to the value of the range error and the angle error. The range error and the angle error matching with the target SNR are conducive to improving performance.

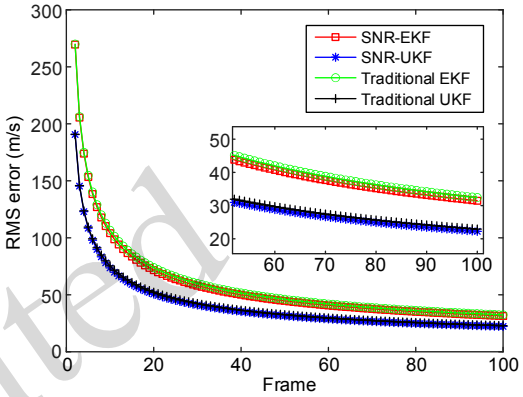

Fig. 15 RMSE of target velocity

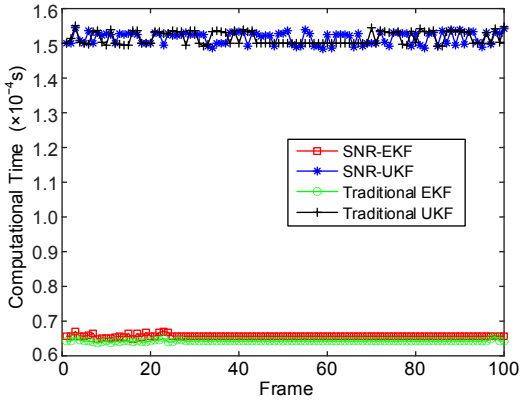

Fig. 16 The computational time of four methods

5 Conclusions

In this paper, the SNR-EKF method and the SNR-UKF method are proposed based on the SNR model. Through simulation analysis, the conclusions are as follow:

1. Compared with the traditional EKF method and the UKF method, the SNR-UKF method and the SNR-EKF method have superior performance (higher prediction accuracy and faster convergence speed)

and little influence on computation time.

2. Compared with the SNR-EKF method, the SNR-UKF method has higher velocity precision, but has longer computation time, and their position precision is almost the same.

Contributors (refer to https://www.casrai.org/credit.html)

Compliance with ethics guidelines

Dai Liu, Yong-bo Zhao, Zi-qiao Yuan, Jie-tao Li, and Guo-ji Chen declare that they have no conflict of interest.

References

Alberhseim WJ, 1981. A closed-form approximation to Robertson's detection characteristics. *Proc IEEE*, 69(7):839. https://doi.org/10.1109/PROC.1981.12082

Barczyk M, Bonnabel S, Deschaud JE, et al., 2015. Invariant EKF design for scan matching-aided localization. *IEEE Trans Control Syst Technol*, 23(6):2440-2448. https://doi.org/10.1109/TCST.2015.2413933

Brekke E, Hallingstad O, Glattetre J, 2010. Tracking small targets in heavy-tailed clutter using amplitude information. *IEEE J Oceanic Eng*, 35(2):314-329. https://doi.org/10.1109/JOE.2010.2044670

Brekke E, Hallingstad O, Glattetre J, 2011. The modified Riccati equation for amplitude-aided target tracking in heavy-tailed clutter. *IEEE Trans Aerosp Electron Syst*, 47(4):2874-2886. https://doi.org/10.1109/TAES.2011.6034670

Daniyan A, Lambotharan S, Deligiannis A, et al., 2018. Bayesian multiple extended target tracking using labeled random finite sets and splines. *IEEE Trans Signal Proc*, 66(22):6076-6091. https://doi.org/10.1109/TSP.2018.2873537

Das A, Rao BD, 2012. SNR and noise variance estimation for MIMO systems. *IEEE Trans Signal Proc*, 60(8):3929-3941. https://doi.org/10.1109/TSP.2012.2194707

Du L, Liu H, Bao Z, et al., 2007. Radar automatic target recognition using complex high-resolution range profiles. *IET Radar Sonar Nav*, 1(1):18-26. https://doi.org/10.1049/iet-rsn:20050119

Ehrman LM, Lanterman AD, 2008. Extended Kalman filter for estimating aircraft orientation from velocity measurements. *IET Radar Sonar Nav*, 2(1):12-16. https://doi.org/10.1049/iet-rsn:20070025

Ehrman LM, Mahapatra PR, 2009. Impact of noncoherent pulse integration on RCS-assisted tracking. *IEEE Trans Aerosp Electron Syst*, 45(4):1573-1579. https://doi.org/10.1109/TAES.2009.5310319

Gokce M, Kuzuoglu M, 2015. Unscented Kalman filter-aided Gaussian sum filter. *IET Radar Sonar Nav*, 9(5):589-599. https://doi.org/10.1049/iet-rsn.2014.0088

Hong L, Wu S, Layne JR, 2004. Invariant-based probabilistic target tracking and identification with GMTI/HRR measurements. *IEE Proc Radar Sonar Nav*, 151(5):280-290. https://doi.org/10.1049/ip-rsn:20040858

Liu CY, Shui PL, Li S, 2011. Unscented extended Kalman filter for target tracking. *J Syst Eng Electron*, 22(2):188-192. https://doi.org/10.3969/j.issn.1004-4132.2011.02.002

Liu D, Zhao YB, Xu BQ, 2019. Tracking algorithms aided by the pose of target. *IEEE Access*, 7:9627-9633. https://doi.org/10.1109/ACCESS.2019.2890981

Menegaz HMT, Ishihara JY, Kussaba HTM, 2019. Unscented Kalman filters for riemannian state-space systems. *IEEE Trans Automat Control*, 64(4):1487-1502. https://doi.org/10.1109/TAC.2018.2846684

Mertens M, Ulmke M, Koch W, 2016. Ground target tracking with RCS estimation based on signal strength measurements. *IEEE Trans Aerosp Electron Syst*, 52(1):205-220. https://doi.org/10.1109/TAES.2015.140866

Musicki D, Song TL, 2013. Track initialization: prior target velocity and acceleration moments. *IEEE Trans Aerosp Electron Syst*, 49(1):665-670. https://doi.org/10.1109/TAES.2013.6404131

Rashedi M, Liu JF, Huang B, 2018. Triggered communication in distributed adaptive high-gain EKF. *IEEE Trans Ind Inform*, 14(1):58-68. https://doi.org/10.1109/TII.2017.2715340

Ruan Y, Hong L, 2006. Feature-aided tracking with GMTI and HRR measurements via mixture density estimation. *IEE Proc Control Theory Appl*, 153(3):342-356. https://doi.org/10.1049/ip-cta:20045099

Skolnik M, 2010. Introduction to Radar System. Publishing House of Electronics Industry, Beijing, China.

Tang X, Tharmarasa R, McDonald M, et al., 2017. Multiple detection-aided low-observable track initialization using ML-PDA. *IEEE Trans Aerosp Electron Syst*, 53(2):722-735. https://doi.org/10.1109/TAES.2017.2664598

Tufts DW, Cann AJ, 1983. On Albersheim's detection equation. *IEEE Trans AES*, AES-19(4):643-646. https://doi.org/10.1109/TAES.1983.309356

Villano M, 2014. SNR and noise variance estimation in Polarimetric SAR data. *IEEE Geosci Remote Sens Lett*, 11(1):278-282. https://doi.org/10.1109/LGRS.2013.2255860

Xi YH, Zhang XD, Li ZW, et al., 2018. Double-ended travelling-wave fault location based on residual analysis using an adaptive EKF. *IET Signal Proc*, 12(8):1000-1008. https://doi.org/10.1049/iet-spr.2017.0486

Zhang XY, Huang JL, Wang GH, et al., 2019. Hypersonic target tracking with high dynamic biases. *IEEE Trans Aerosp Electron Syst*, 55(1):506-510. https://doi.org/10.1109/TAES.2018.2884187

Zhang Y, Mu HL, Jiang YC, et al., 2019. Moving target tracking based on improved GMPHD filter in circular SAR system. *IEEE Geosci Remote Sens Lett*, 16(4):559-563.

https://doi.org/10.1109/LGRS.2018.2878467

Zhou GJ, Pelletier M, Kirubarajan T, et al., 2014. Statically fused converted position and Doppler measurement Kalman filters. *IEEE Trans Aerosp Electron Syst*, 50(1):300-318. https://doi.org/10.1109/TAES.2013.120256